Homology Modeling of NR2B Modulatory Domain of NMDA Receptor and Analysis of Ifenprodil Binding

Luciana Marinelli,*[a] Sandro Cosconati,[a] Thomas Steinbrecher,[b] Vittorio Limongelli,[a] Alessia Bertamino,[a] Ettore Novellino,[a] and David A. Case[b]

NMDA receptors are glutamate-gated ion channels (iGluRs) that are involved in several important physiological functions such as neuronal development, synaptic plasticity, learning, and memory. Among iGluRs, NMDA receptors have been perhaps the most actively investigated for their role in chronic neurodegeneration such as Alzheimer's, Parkinson's, and Huntington's diseases. Recent studies have shown that the NTD of subunit NR2B modulates ion channel gating through the binding of allosteric modulators such as the prototypical compound ifenprodil. In the present paper, the construction of a three-dimensional model for the NR2B modulatory domain is described and docking calculations allow, for the first time, definition of the ifenprodil binding pose at an atomic level and fully explain all the available structure–activity relationships. Moreover, in an attempt to add further in-

sight into the ifenprodil mechanism of action, as it is not completely clear if it binds and stabilizes an open or a closed conformation of the NR2B modulatory domain, a matter, which is fundamental for the rational design of NMDA antagonists, MD simulations followed by an MM-PBSA analysis were performed. These calculations reveal that the closed conformation of the R1-R2 domain, rather than the open, constitutes the high affinity binding site for ifenprodil and that a profound stabilization of the closed conformation upon ifenprodil binding occurs. Thus, for a rational design and/or for virtual screening experiments, the closed conformation of the R1-R2 domain should be taken into account and our 3D model can provide valuable hints for the design of NR2B-selective antagonists.

Introduction

Ionotropic glutamate receptors (iGluRs) are glutamate-gated ion channels that have been classified into three subtypes, according to their sensitivity to the agonists NMDA (N-methyl-D-aspartate), AMPA (α-amino-3-hydroxy-5-methyl-4-isoxazole propionic acid), and kainate (a structural analogue of glutamate).[1] These ion channels are involved in several important physiological functions such as neuronal development, synaptic plasticity, learning, and memory.[2] Among iGluRs, the NMDA receptors have been perhaps the most actively investigated for their role in chronic neurodegeneration. Excessive activity of NMDA receptors have been associated with ischemic brain injury/stroke, chronic/neuropathic pain states, Alzheimer's, Parkinson's, and Huntington's diseases.[3] The pivotal role of NMDA receptors in mediating pain and multiple neurodegenerative disorders, together with the limited treatment options currently available for these diseases, have been the driving force in the search of safe and effective drugs that target this system.

From a structural point of view, NMDA receptors are thought to be heterooligomers that are composed of two glycine-binding NR1 subunits (eight different splice variants exist), which combines with one or more glutamate-binding NR2 subunits (types A–D).[4] Co-expression of NR1 with one or more of the NR2 subunits yields receptors with distinct functional and pharmacological properties.[5] Up to now, many endogenous
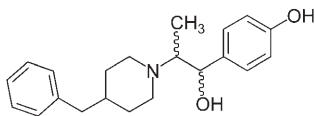
and exogenous ligands, acting as agonists or antagonists have been described to interact with NMDA receptor at distinct sites. Unfortunately, ligands binding at the glutamate and glycine sites have shown low selectivity against the different subtypes of NMDA receptors, resulting in several adverse central nervous system (CNS) effects, which have dramatically hampered their therapeutic utility so far.[6]

The continuous advances in our understanding of the molecular structure of the NMDA receptor have led pharmaceutical researchers to investigate the possibility of developing subtype-selective blockers of the NMDA receptor in an effort to separate the efficacious profiles from the adverse ones. Of particular interest are the NR2B-containing NMDA receptor channels, as an overstimulation of such receptors is known to pro-

[a] *Prof. L. Marinelli, Dr. S. Cosconati, Dr. V. Limongelli, Dr. A. Bertamino,*
 Prof. E. Novellino
 Dipartimento di Chimica Farmaceutica e Tossicologica
 Università di Napoli "Federico II"
 Via D. Montesano 49, 80131 Napoli (Italy)
 Fax: (+39) 081-678139
 E-mail: lmarinel@unina.it

[b] *Dr. T. Steinbrecher, Prof. D. A. Case*
 Department of Molecular Biology
 The Scripps Research Institute
 10550 North Torrey Pines Road, La Jolla, CA 92037 (USA)

mote neuronal death and dysfunctions such as Alzheimer's and Parkinson's diseases or epilepsy. As the observation that ifenprodil, a well-known antagonist of the α1-adrenergic re-

ceptor, exhibited a higher affinity towards NR2B than for NR2A subunits (400-fold),[7] great efforts have been made to find new "ifenprodil-like" compounds targeting NR2B-containing NMDA receptors.

The recent available preclinical and clinical data are encouraging, demonstrating that NR2B-selective antagonists are better tolerated than previous classes of NMDA blockers, while retaining efficacy equivalent to, or better than, previous nonselective compounds. Nevertheless, the great majority of these compounds are burdened with poor pharmacokinetic performances. Thus, new potent NR2B-selective antagonists are still in great demand. So far, high-throughput screening and SAR studies have been the major sources of new antagonists, whereas computer-aided drug design methods have been long hampered both by the absence of any X-ray structure of NMDA and by the lack of any information on the location of the ifenprodil binding site within NR2B. Despite the lack of any X-ray structure of the NR2B subunit, it is well known that it shares a common membrane topology with other iGluR subunits[1] being made of a large extracellular N-terminal domain (NTD), a transmembrane region (helices I, III, IV) that constitutes the ion pore, a re-entrant loop (II) that forms the selectivity filter, and a cytoplasmic C-terminal domain that interacts with intracellular components (Figure 1).

More precisely, the NTD consists of two bi-lobed domains, one of which is made of the first 380 residues (R1-R2) and has structural similarity with the bacterial periplasmic leucine, isoleucine, valine binding protein (LIVBP).[8] This domain is particularly important as it contains the binding sites for the endogenous modulators of NMDA activity such as zinc ions, polyamines, and protons.[8] The other domain, made of ~150 amino acids (S1-S2), is distantly related to the bacterial periplasmic glutamine binding protein (GlnBP) and forms the agonist binding site.[9]

For a long time, the precise position of the ifenprodil binding site has remained elusive until site-directed mutagenesis experiments unambiguously located it to the LIVBP-like domain of the NR2B subunit.[10] Recently, experimental evidence demonstrated that ifenprodil competes with Zn^{2+} for the binding to the NTD of the NR2B subunit, thus proving that this ion would be the endogenous ligand of the above-cited domain.[11] Currently, the availability of the X-ray coordinates of several LIVBP-like domains on the one hand, and of functional studies of ifenprodil–NR2B interactions, on the other hand, allowed the building, through the comparative modeling technique, of the NR2B modulatory domain three-dimensional structure and the computational exploration of ifenprodil–
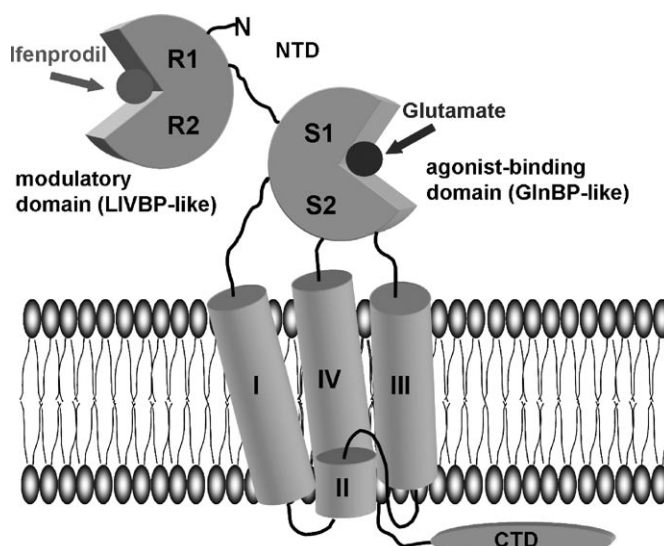
Figure 1. Topology of the NMDA receptor NR2B subunit. The NR2B subunit is made of a N-terminal domain (NTD) comprising a modulatory, or regulatory (R1-R2) LIVBP-like domain, and a GlnBP-like domain (S1-S2) which binds the agonist L-glutamate, a transmembrane domain, made of three membrane spanning segments (I, III, and IV) that forms the pore together with a re-entrant loop (II), and finally a cytoplasmic C-terminal domain (CTD) that interacts with intracellular components.

NR2B interactions at the atomic level. Herein, we present the first three-dimensional model of the NR2B–ifenprodil complex, which can provide valuable hints for the design of NR2B-selective antagonists. The model, whose coordinates will be available upon request, could also be used for virtual screening experiments.

Finally, in the attempt to add further insight into the ifenprodil mechanism of action, molecular dynamics calculations followed by a molecular mechanics Poisson–Boltzmann/surface area (MM-PBSA) analysis was undertaken.

Results and Discussion

Sequence analysis and homology modeling of NR2B modulatory domain

In the case of NMDA receptors, functional experiments have established that ifenprodil binds to the R1-R2 domain of NR2B and modulates ion-channel gating by an allosteric mechanism.[10] As regards the R1-R2 domain structure, strong evidence exists that it has similar folding to the bacterial leucine-isoleucine-valine-binding protein (LIVBP) and to the agonist-binding domain in G-protein-coupled glutamate receptors (mGluRs).[10]

The general concept that the ligand-binding domain of vertebrate glutamate receptor channels and various bacterial periplasmic substrate-binding proteins (PBPs) share similar three-dimensional (3D) structures has gained increasing support in recent years. In fact, a review article concerning to what extent theoretical models have predicted the crystal structure of the ligand-binding domain of glutamate receptors shows that de-

spite the low sequence identity with the templates used, molecular modeling has been successful in the structure prediction.[12] This finding once more suggests that a phylogenetically conserved amino acid binding fold creates the binding pockets of diverse types of glutamate receptors.

However, the NMDA R1-R2 domain is expected to be slightly distinct from the structure of the agonist-binding core of iGluRs because in LIVBP and mGluRs, the two globular domains are connected by three loops instead of the two β-strands found in the iGluR glutamate- and glycine-binding cores. As a result of the low sequence identity between the NMDA R1-R2 domain and LIVBP or mGluRs (see Experimental Section), a multiple sequence alignment generated by for example, the ClustalW program would not be meaningful. Therefore, we had the benefit of an HCA-based sequence alignment (see Experimental Section and Figure 2) that has been previously performed by Paoletti et al. and subsequently validated through functional studies of ifenprodil–NR2B interactions.[10]

An analysis of X-ray structures of the two possible templates (LIVBP and mGluR1), clearly showed that the LIVBP-like domain undergoes, upon ligand binding, a conformational change from an open to a closed form. In particular for LIVBP, an unligated-open form, an unligated-"superopen" form, an open ligand-bound form, and three closed conformations complexed with leucine, isoleucine, or valine have been reported.[13] Similarly for mGluR1, X-ray structures of the unligated open, ligated open, and ligated closed forms have been recently obtained.[14] The superposition of the Cα atoms in the LIVBP and mGluR1 ligand binding region (LBR) led to an RMSD of only 1.8 Å demonstrating a common architecture despite the low sequence identity (17%). In the homology modeling procedure, mGluR1 was used as the reference structure. This template has been crystallized as a homodimer. Both proto-

mers (A and B) consist of two globular lobes with α/β folds, interconnected by a hinge region, made of three connecting loops, that permits a rigid body lobe closure upon ligand binding.[14] The two protomers differ in the degree of lobe closure and were respectively used to generate twelve models for the closed and twelve models for the open conformation of the NR2B modulatory domain.

Thus, the Modeller Program was used to generate an ensemble of alternative conformations to take into account different residue side-chain conformations and the expected structural flexibility of the loops. Generation of alternative loop models is particularly important for the success of the following docking experiments as in both, LIVBP and mGluR1, residues known to contact the ligand belong mostly to the loops connecting the two globular subdomains.

Thus, building of the R1-R2 domain results in a total of forty models, all presenting the domain divided into two globular lobes (here referred to as lobe I and lobe II or R1 and R2) with an alternation of β strands and α helices. Analogously to mGluR1, the three segments linking the two domains (loops β5/α5, β10/α10, β11/β12) although widely separated in the primary sequence (see alignment), are in close proximity in the tertiary structure and form the hinge necessary for interdomain motion known to be crucial in signal transmission. Whereas interdomain loops β5/α5 and β11/β12 extend from lobe I to lobe II, loop β10/α10 runs in the opposite direction. Loops β5/α5 and β10/α10 are preceded by a β-sheet strand in one domain and followed by an α-helix in the other domain, whereas loop β11/β12 bridges strands from both domains. In the twenty open forms, the two domains are well separated, and the cleft between the two domains is wide open and accessible to solvent. In contrast, in the closed forms the lips of the two domains are nearly in contact.
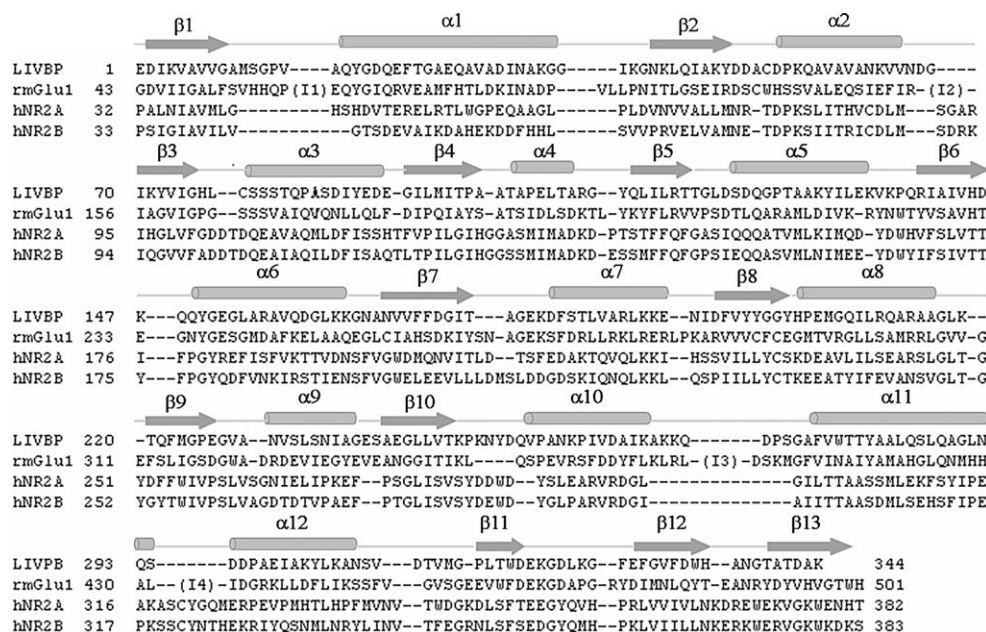

Figure 2. Multiple amino acid sequence alignment of the LIVBP-like domain of the human NMDA NR2A-B subunits with LIVBP-like domains of LIVBP from *E. coli* and of mGluR1 from rat. The β strands (arrows), α helices (boxes), identified in the LIVBP and mGluR1 crystal structures are indicated on top of the alignment. The large insertions found in mGluR1 with respect to LIVBP have been removed and are indicated by I1 to I4.

With respect to the structure of the template (mGluR1), the R1-R2 domain of NR2B primarily differed in the absence of four loops denoted as I1–I4 (insertion) in the sequence alignment (Figure 2). Interestingly, in mGluR1, all four loops are in lobe I and two of them (I1, I3) are close to the ligand binding site. In particular, the loop corresponding to insertion I1 lies over the binding site for glutamate narrowing access to that region, whereas the loop resulting from insertion I3 is in between α10 and α11 and strongly protrudes out from lobe I. Comparing the two binding clefts (mGluR1, NMDA), there is a great number of amino acid changes in the loops lining the binding sites, thus imparting specific substrate recognition.

The superposition of the multiple generated models of R1-R2, helps to better detect the flexible regions of the constructed domain (Figure 3). As regards the closed models, the twenty conformations mainly differ in the α11/α12, β12/β13, α12/β11 loop conformations. However, especially for α11/α12 and β12/β13 loops, they should not affect the ligand binding all being far enough from the central cleft thought to be the ligand binding site. In this respect, the differences observed for the β3/α3, β4/α4, β9/α9 loop structures, which are all located in the central cleft and contain residues known to contact ligands in the template proteins are more significant.[13, 14] As regards the residues lining the cleft, an expected flexibility in the residue side-chain conformation was also found.

Comparing the superposition of all open structures to that of all closed conformations (Figure 3a and b), it emerges that among the open conformations a larger variability exists with respect to the closed forms. For example, the β10/α10 loop seems to be more flexible when considering the open conformations with respect to the closed. This is probably due to less tight packing in the open form.

With the aim of locating the ifenprodil binding site for subsequent docking studies (AutoDock allows the positioning of a box around the putative binding site in which all the calculations will be performed), all mutagenesis data available for the NMDA receptor were taken into account, together with knowledge about the ligand-binding region of homologous proteins such as LIVBP and mGluR1. Mapping of residues recently detected as important for NR2B–ifenprodil binding, into our 3D models of the modulatory domain, shows that they belong to both lobes, and are mainly located in regions lining the central cleft.[10] This suggests, as in the case of Leu, Ile, and Val for LIVBP or glutamate for mGluR1, that ifenprodil binds in the cleft of the LIVBP-like domain of NR2B, consistent with the observations of Gallagher et al.,[15] who found that the N-terminal region of NR2B controls the high-affinity ifenprodil inhibition. Notably Masuko et al.,[16] found that some mutations in the LIVBP-like domain of NR1 also affect ifenprodil sensitivity of the NR1/NR2B dimer. However, this apparent discrepancy has to be reconsidered in the light of all the dimeric structures available for LIVBP-like domains. In fact, although in the case of the NR1/NR2 NTD dimer, a crystal structure is not available at the moment, clues of possible dimerization modes can be inferred from the structures of the LIVBP-like domains of rat mGluR1 and ANP-C, crystallized as homodimers.[13, 17] In both X-Ray structures, the LIVBP-like domains dimerize in a "back-to-back" fashion. Interestingly, an analysis of sequence alignments between NMDA-NR1, mGluR1, and ANP-C LIVBP-like domains shows that the residues of NMDA-NR1 identified by Masuko et al. coincide with residues located at the dimer interface in mGluR1 and ANP-C. Therefore, it is likely that the residues identified on NR1, rather than being directly involved in contacting ifenprodil, reside in the interface between two LIVBP-like domains (NR1/NR2B) and are certainly important for the gating machinery involved in the ifenprodil-induced conformational change in the NR2B LIVBP-like domain. Based on these considerations, ifenprodil was automatically docked by means of the AutoDock program both in the open and closed form of the NR2B modulatory domain. To partially overcome the limitations of the rigid protein approach applied in the docking program, ifenprodil was docked in an ensemble of R1-R2 conformations generated by MODELLER. In this way, diverse loop models together with different orientations of binding site residues can be taken into consideration during the ligand docking process. To reduce the computational time, without belittling the meaning of the ensemble docking, ten of the twenty models of the open and ten of the closed conformations were selected for the subsequent ligand docking studies. Only the R1-R2 models meeting
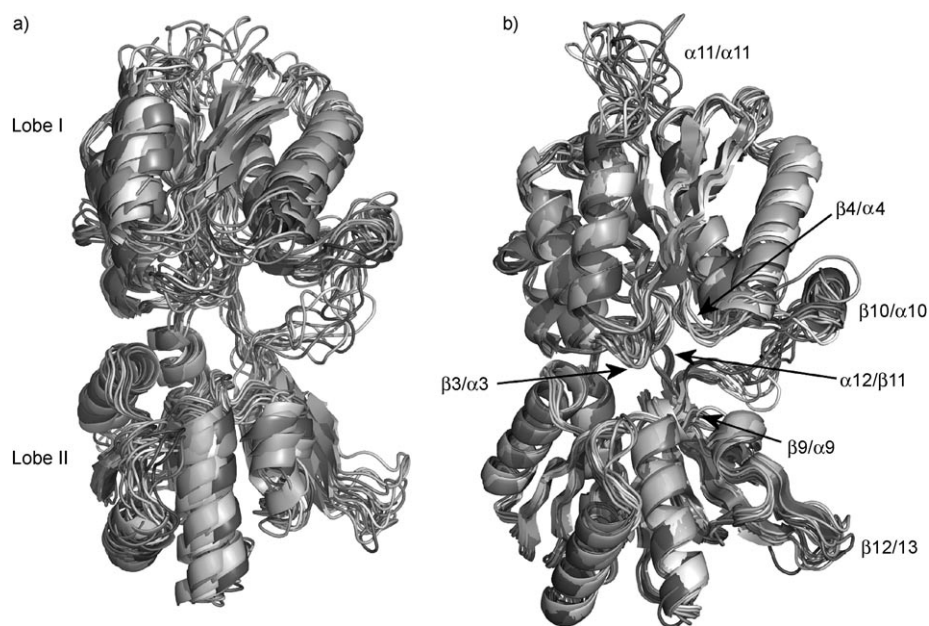

Figure 3. Backbone superposition of the ten homology models selected to represent the R1-R2 domain in the a) open and in the b) closed conformation. A certain variability in the loops segments is displayed.

the following criteria were retained for further calculations: 1) models presenting differences in the shape of β3/α3 loop or substantial variation in the side-chain conformation of D101, T103, D104; 2) models presenting differences in the shape of β6/α6 loop or considerable differences in the side-chain conformation of F176; 3) models presenting dissimilarity in the shape of β8/α8 loop or relevant differences in the side-chain conformation of T233 or K234. The rationale for this model selection is supported by mutagenesis experiments, which suggest the above-mentioned loops and residues as ifenprodil interacting regions.

The ensemble docking approach helps to establish which of the constructed models is the most reliable one, being able to bind the ifenprodil ligand consistently with protein mutagenesis data and ligand SARs.

Table 1. Comparison of the ifenprodil enantiomers.

| Configuration | IC$_{50}$ ± SEM [nM] (n)[a] | | |
	CC	α1	TI
(+)-*erythro* racemic	263 ± 63 (4)	100 ± 36 (5)	0.38
(+)-*erythro*	NT	NT	–
(−)-*erythro*	110 ± 39 (4)	135 ± 35 (3)	1.23
threo racemic	55 ± 13 (3)	843 ± 137 (3)	15.3
(+)-*threo*	48 ± 18 (3)	2306 ± 850 (3)	48.0
(−)-*threo*	13,3 ± 1,7 (3)	629 ± 297 (3)	47.3

[a] The activity was measured in rat hippocampal cell cultures by observing the ability of the compounds to protect the cultured neurons from the toxic effects of extracellularly applied glutamate. This glutamate-induced hippocampal neurodegeneration model is referred to as the cell culture model (CC). The ratio of potencies at α1 adrenergic receptors versus CC activity will be used as a measure of selectivity (therapeutic ratio, TI). NT = not tested. Table extracted from Ref. [19]; see it for more details.
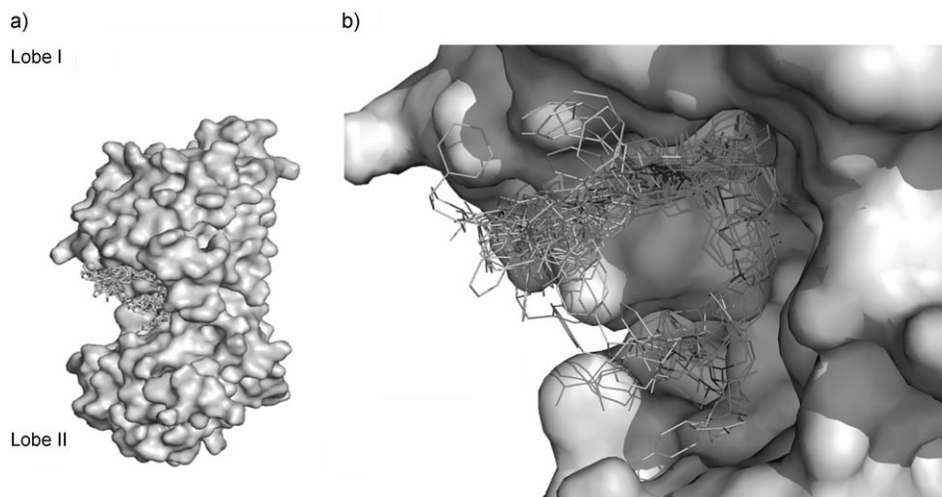
Docking of ifenprodil into the NR2B modulatory domain

Biological activity of both the (±)-*erythro* and (±)-*threo* ifenprodil was first measured in rat hippocampal cell cultures, by observing the ability of the compounds to protect the cultured neurons from the toxic effects of extracellularly applied glutamate.[19] This study demonstrated that (±)-*threo* ifenprodil was about five times more active than (±)-*erythro* ifenprodil at preventing glutamate-induced hippocampal neuronal death (see Table 1). Subsequent studies, based on voltage-clamp recording,[18] were only partially in accordance with those previously obtained[19] as no difference in potency between (±)-*erythro* and (±)-*threo* ifenprodil

Figure 4. Connolly surface of R1-R2 domain in an open conformation. a) A total of 43 out of 50 runs docked ifenprodil attached to lobe I and a considerable number of solutions was found near to D101 (not shown) known experimentally to interact with ifenprodil. b) On the right side, a close-up view of the 50 solutions proposed by the docking program.

at the NR1A/NR2B subunit combination was observed.[18] However, the (±)-*threo* ifenprodil displayed a significantly reduced α1 activity[19] and subsequent studies conducted on a close analogue of ifenprodil clearly show that the (1S,2S)-enantiomer is the one endowed with greater separation of NMDA and α1 adrenergic activities.[20] Therefore, in our study, we decided to dock ifenprodil, with a *threo* stereochemistry and with a 1S,2S absolute configuration to both the open and closed conformations of the R1-R2 domain.

It is interesting to note that when docking experiments were performed on each open model, in almost all solutions proposed by the program, ifenprodil exclusively binds to lobe I. As shown in Figure 4, of the 50 binding poses proposed, in none of them does ifenprodil bind both lobes at the same time. Such a result is in line with the observation that in the open conformation of LIVBP or mGluR1 bi-lobed domains, only lobe I participates in ligand binding.[13,14] Differing from the

LIVBP ligands which are uncharged amino acids, and from the mGluR1 physiological ligand glutamate which is negatively charged, ifenprodil is thought to be positively charged in its interaction with the NR2B subunit. Accordingly, in the match between the two different lobes of NR2B, it seems likely that the one exposing more negatively charged residues on its surface (lobe I: D101, D102, D104, E106) prevails over the other in binding ifenprodil.

As expected, docking results were sensitive to the different domain conformations and not all homology models were able to bind ifenprodil consistently with the mutagenesis and ifenprodil SAR data. For example, regarding the set of open conformations, some models showed that ifenprodil is anchored to lobe I mainly by a coulombic interaction between the protonated nitrogen of the ligand and the E47 side chain. Such an interaction is present in those models in which E47 orients its side chain toward the center of the cleft, whereas

Table 2. Screening of point mutations in the LIVBP-like domain of NR2B for effects on ifenprodil sensitivity.

	Mean relative current [%]	
NR2B mutant[a]	300 nm ifenprodil	3 μm ifenprodil
wt	37±5	8±2
V42A[a]	84±4	35±4
E47A	39±3	9±1
D101A[a]	99±1	91±2
T103A[a]	84±1	39±1
H127A	32±3	7±2
F176A[a]	95±4	82±5
F182A[a]	97±2	86±4
K234A[a]	86±2	41±6
S260A	43±2	12±1
L261A[a]	76±5	9±2
V262A	50±4	11±1
D265A	39±5	10±1

[a] Mutations resulting in a significant decrease in ifenprodil sensitivity; wt = wild type. Table extracted from Ref. [10a]; see it for more details.

other potential binding residues, such as D101, have their side chains buried into lobe I or partially masked by other residues' side chain. These models were discarded as mutation of E47A did not show any loss of binding for ifenprodil (see Table 2). However, over the ten homology models tested for the open conformation, only five bind ifenprodil in accordance with NR2B mutagenesis studies, indicating that D101 (lobe I) is an essential anchor point (see Table 2).[10]

These binding modes are highly similar, having the ligand placed perpendicularly with respect to the hinge segments and held in place by an electrostatic interaction between the protonated nitrogen of the piperidine ring and the D101 side chain. The chosen model (model 1, Figure 5a) shows the maximum number of interactions, with respect to the other models, and is the most consistent with the mutagenesis studies. Besides D101, a H-bond between the ligand hydroxy group and the V42 backbone CO together with van der Waals interactions between the T103 carbons and the piperidine ring have been observed. Moreover, F99 participates in a T-shaped interaction with the phenol ring of ifenprodil. Consistent with

the above-described binding mode, mutation of D101 led to a complete loss of binding, whereas V42A and T103A mutations had a pronounced effect on ifenprodil sensitivity.[10] However, it has to be noted that the benzyl group of ifenprodil does not find any partner for an aromatic interaction, although SAR studies and the only pharmacophore hypothesis published so far[23] both indicate that two aromatic features of ifenprodil are important for binding and they have to be at an appropriate distance (see Table 3 and 4, compounds **4** and **7**, **13** and **14**, **15** and **16**). An analysis of lobe I shows that apart from F99, no other aromatic amino acids are present among the residues lining the central crevice. At least three aromatic amino acids (F176, F182, Y231), with their side chains exposed to the solvent, and thus available for ligand binding, are present in lobe II. Moreover, the phenolic hydroxy group is surrounded mostly by aliphatic residues with the exception of E47, known not to participate in ifenprodil binding, although evidence exists for an involvement of the phenolic OH in the interaction with the R1-R2 domain (see Table 3, **1** versus **2**, **4** versus **5**).[19, 22, 23] Thus, of all the binding modes found for the open conformations of R1-R2, none seems to be sufficiently in line with protein mutagenesis and ifenprodil SARs.

As regards docking of ifenprodil in the closed conformation of the modulatory domain, a certain difficulty was encountered by the docking program to place the ligand deep in the central clef. At first sight, this seems to be ascribable to the limited space available in the central cleft to locate ifenprodil. However, docking calculations on three of the ten models analyzed were successful in predicting a binding position of ifenprodil comparable to the one found for glutamate and leucine trapped in their proteins.[13, 14] The three calculated complexes are pretty similar and herein, the one for which the predicted ifenprodil–receptor interactions are most consistent with both protein mutagenesis and SAR data is described. These calculations revealed the presence of a well-defined binding pose in which the ligand adapts itself in the crevice formed by the two lobes of the NR2B modulatory domain, establishing several favorable interactions with the protein (Figure 5b). More precisely, the phenol ring is embedded in a rather profound gorge lined by the backbone COs of P259, S260, and L261, and bordered by
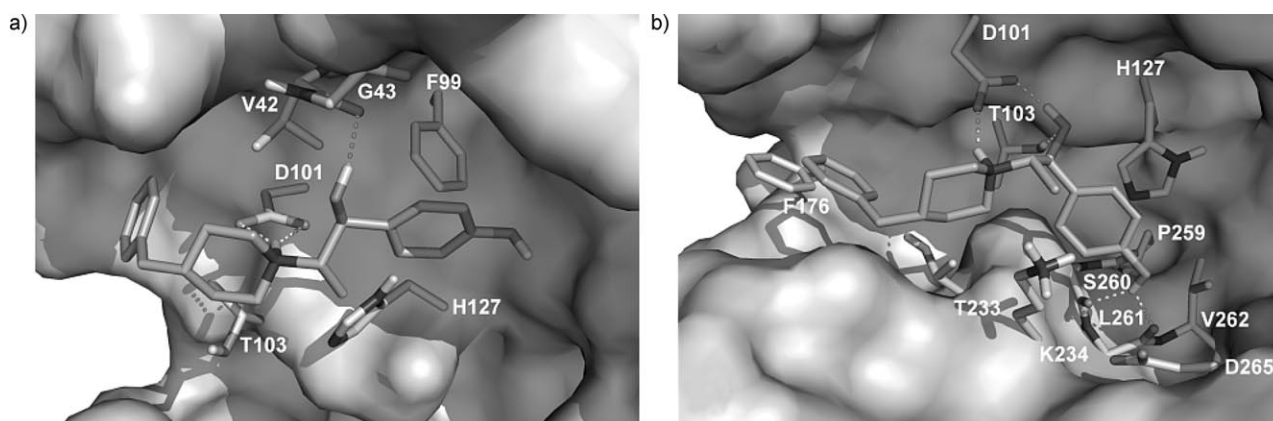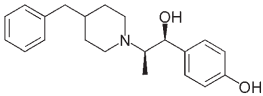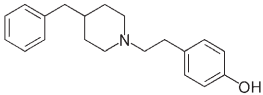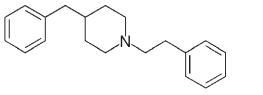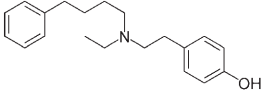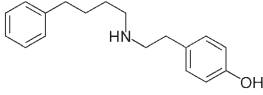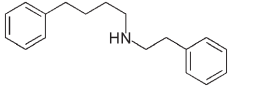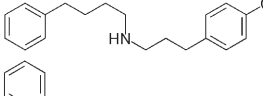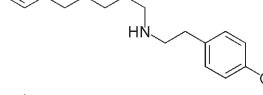

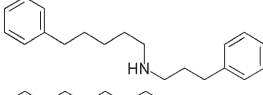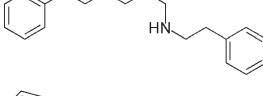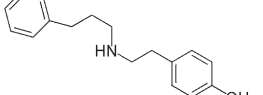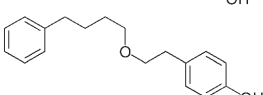**Figure 5.** Binding modes of ifenprodil in the a) open and b) closed conformation of R1-R2 modulatory domain. H-bonds are displayed as dashed lines.
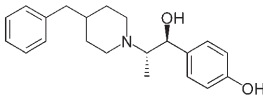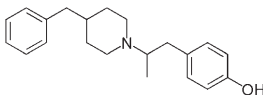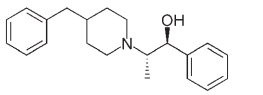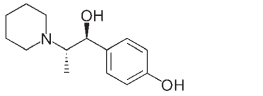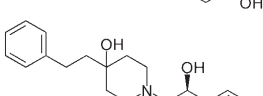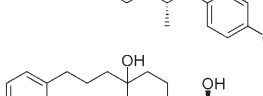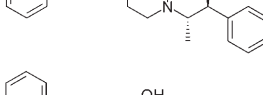
Table 3. Structure–activity relationship of ifenprodil at the NR1A/2B subtype.[a]

Entry	Structure	IC$_{50}$ [μM]
ifenprodil		0.11
1		0.20
2		1.1
3		0.30
4		0.043
5		3.5
6		0.015
7		0.008
8		0.045
9		0.041
10		0.096
11		3.7

[a] Potency is assayed by electrical recordings under steady-state conditions in *Xenopus* oocytes expressing the binary combination (NR1A expressed in combination with NR2B) of cloned rat NMDA receptor subunits. Table extracted from Ref. [23]; see it for more details.
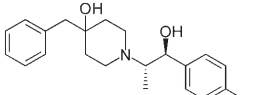
Table 4. Structure–activity relationship of Ifenprodil at the NR1A/2B subtype.

Entry	Structure	IC$_{50}$ [nM]
ifenprodil *threo*[b]		55 ± 13 $n=3$
12[a]		153 ± 3 $n=3$
13[a]		3700 ± 700 $n=3$
14[a]		> 10 000 $n=2$
15[b]		58 ± 17 $n=4$
16[b]		1.3 ± 0.5 $n=3$
17[b]		15.7 ± 3.9 $n=3$
18[b]		1000 $n=2$

[a] The activity was measured in rat hippocampal cell cultures by observing the ability of the compounds to protect the cultured neurons from the toxic effects of extracellularly applied glutamate. For ifenprodil enantiomer activities, please refer to Table 1. Data extracted from Ref. [19]; see it for more details. [b] The potency was measured for inhibition of glutamate-induced neuron death in primary cultures of rat hippocampal neurons. Data extracted from Ref. [20]; see it for more details.

H127, V262, and D265 side chains. In this cleft the phenol ring was found to establish a cation–π interaction with K234 and optimally oriented to H-bond with both the backbone COs of S260 and L261. Indeed, the above cited gorge is characterized by the presence of several H-bond accepting groups and possibly the ligand phenolic OH could alternatively interact with each of them. The implication of the phenolic hydroxy group in ligand binding was also outlined by SAR studies indicating that its removal results in weaker ligands than ifenprodil at NR1A/2B receptors (see Table 3, **1** versus **2**, **4** versus **5**).[19, 22, 23] In contrast to the phenolic hydroxy group, the ligand hydroxyl group is involved in a network of H-bonds acting as an acceptor with the T103 side chain and as a donor with the D101 side chain (Figure 5b). The implication of the above mentioned residues in the binding of ifenprodil are in perfect accord with mutagenesis experiments in which mutations T103A, K234A, and L261A have pronounced effects on ifenprodil sensitivity (see Table 2).[10] The interaction of ifenprodil with the D101 residue is also characterized by the presence of a charged-reinforced H-bond between the protonated amino group of the ligand and the side chain of D101 (Figure 5b). The involvement of the latter residue in a double interaction with ifenprodil might explain why replacement of this amino acid with an alanine completely abolishes ligand binding (see Table 2).[10] All ifenprodil analogues published to date display the presence of a protonated amine group, with the exception of compound

11 (see Table 3), for which a deep decrease of activity was found (**4** versus **11**). Moreover, SAR data indicate that ifenprodil analogues featuring a secondary instead of a tertiary amine are more potent (Table 3, see **1**, **3**, **4**).[23] Indeed, such an increase in potency can be attributed to the less hindered nature of the basic nitrogen providing a more effective electrostatic interaction with D101. The role of the basic nitrogen atom between the two aromatic rings has long been considered critical for the affinity of a ligand to the NR2B NTD. However, the recent identification of compounds, termed "ifenprodil-non-like" because of the absence of the protonated nitrogen, demonstrates that the basic nitrogen between the two aromatic ring is not mandatory for selective NR2B binding.[24] Accordingly, in the present model the existence of two attachment points (the basic nitrogen and the benzylic OH) to the crucial D101 would explain why the removal of one of them does not cause a loss of antagonist activity towards NMDA.

Interestingly, the calculated posing also allows the nonphenolic ring of the ligand to establish an off-center parallel displaced π–π interaction with the F176 side chain (Figure 5b) in accordance with mutagenesis data that indicated that it is another essential residue for ifenprodil binding (Table 2).[10] In our model the distance between the centroids of the two aromatic rings is 5.5 Å, thus it would be reasonable to think that an extension of the spacer between the nitrogen atom and the nonphenolic ring would lead to a reinforcement of the π-stacking found. A detailed analysis of the SARs available for ifenprodil analogues confirms our hypothesis (see Table 3, **4** versus **7** and **15** versus **16**).[20, 23] From the same SAR studies it emerges that shortening of the above mentioned chain or a too profound extension resulted in a reduction in potency,[23] thus confirming the importance of a proper distance for a π interaction between the two aromatic rings (**7** versus **10** and **7** versus **9**).

Mapping all residues known to affect ligand binding in the 3D structures of the two complexes (Figure 6) clearly shows that they are located on both lobes and according to our open and closed models, these residues are rather distant in the open conformation (for example, one of the shortest distances is the one between the D110 Cγ and the centroids of F176 is

Figure 6. 3D models of LIVBP-like domain (R1-R2) represented as ribbon. The residues identified as critical for high-affinity ifenprodil inhibition are displayed in dark gray space fill representation (lobe I: Val42, Asp101, Thr103, Asp104, Glu106; lobe II: Phe176, Phe182, Thr233, Lys234, Glu236 Leu261, Gly264, hinge: Ile150). Ifenprodil ligand is shown as light gray space fill spheres.

~13 Å), yet forming a well-defined binding site in the closed conformation of R1-R2.

Considering the binding positions of ifenprodil in the two models (Figure 5), it clearly emerges that while in the open conformation, the ligand establishes a limited number of interactions with the protein being partially exposed to the solvent, but in the closed one, ifenprodil is largely surrounded by residues known to be important for the binding and the number of ligand–protein interaction is maximized. From this point of view, the binding mode found in the closed, if compared to that found in the open conformation of the modulatory domain, turns out to be more in line with protein mutagenesis experiments.

On the other hand, these considerations do not exclude a potential binding of ifenprodil to the open conformation of the protein. Thus, MD and MM-PBSA calculations were performed to add further insight into ifenprodil binding to the open as well as to the closed conformation of the NR2B modulatory domain.

MD and MM-PBSA calculations

Six systems were set up for MD simulations (open and closed R1-R2, the two complexes, two ligand structures in their predicted binding conformations) and subsequently a molecular mechanics Poisson–Boltzmann/surface area (MM-PBSA) analysis was performed. Inspection of the conformational behavior of each system revealed that the MD density and temperature relaxation, yielded equilibrated structures with RMSD values compared to the starting structures of approximately 3 Å for the complex and receptor species and < 2 Å for the solvated ligand. MD simulations in the NPT ensemble were then performed for the complex and receptor species until stable conformations with near constant RMSD values were reached. For the open and closed complex structures as well as for the closed receptor structure, 400 ps of additional equilibration time were performed, whereas for the open conformation of the receptor, 1 ns of equilibration was needed. Starting from the first stable structure of each species, structural snapshots for MM-PBSA evaluation were saved in 10 ps time intervals for a total of 100 snapshots for each of the six systems. The average all-atom RMSD value of the open and closed complexes during this 1 ns production phase was 4.8 Å and 4.2 Å, respectively. Comparable all-atom RMSD values were also found for the open and closed receptor (4.4 Å and 4.1 Å, respectively) with the backbone RMSD values being 0.5–1.0 Å smaller (Figure 7).

As regards the closed conformation complex, all the secondary structures preserved their folding and the main differences between the starting structure and the final one especially resided in the β1-α1, β7-α7, α8-β8, β9-α9 loop conformations. Similarly, for the open complex, a major flexibility is observed in the α1-β1, β4-α4, α10-α11, β10-α10, α11-α12, α12-β11 loops.

Plotting the B-values from mass-weighted averaged backbone atom positional fluctuation allows detection of the mobility of each residue during the MD simulations (Figure 8). Inter-
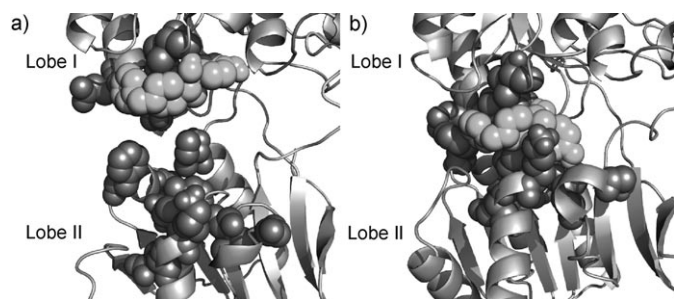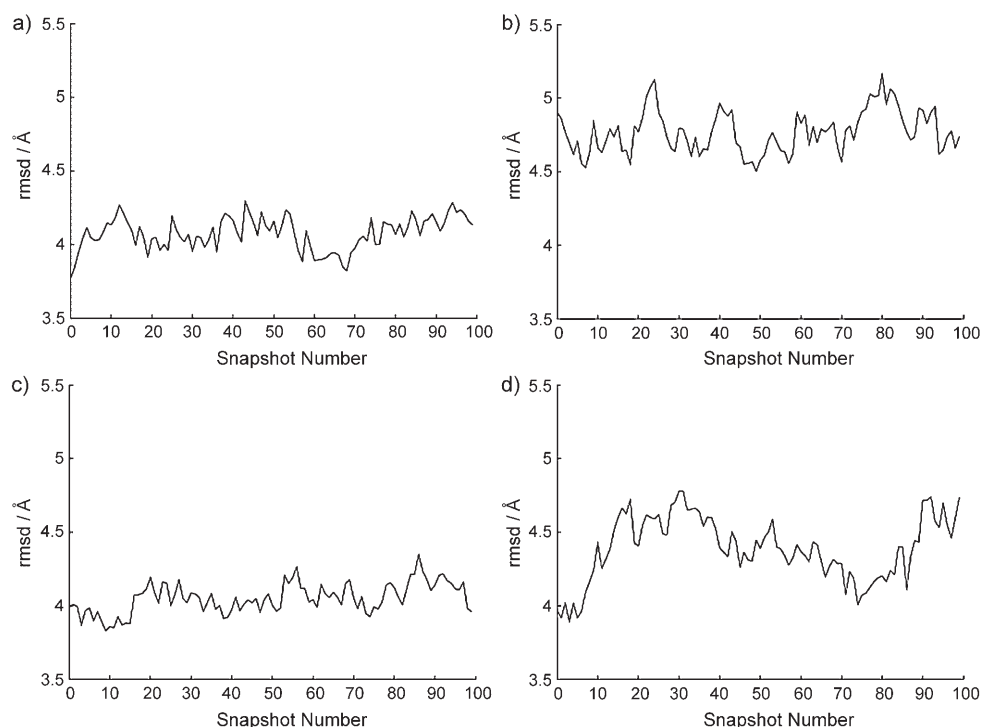
Figure 7. All-atom RMSD in Å of solvated NMDA receptor molecules for the 100 snapshots used in the MM-PBSA calculations. Each plot is equal to a 1 ns MD simulation of a fully equilibrated system (see text). The four plots correspond to the protein ligand complex in the a) closed conformation and b) open confor-mation; as well as the ligand-free receptor in the c) closed conformation and d) open conformation. All systems show stable RMSD values over the full range of the MD simulations, a prerequisite for a meaningful MM-PBSA analysis. Plots for the solvated ligand are not shown, their RMSD values are below 2 Å for the whole simulation time.
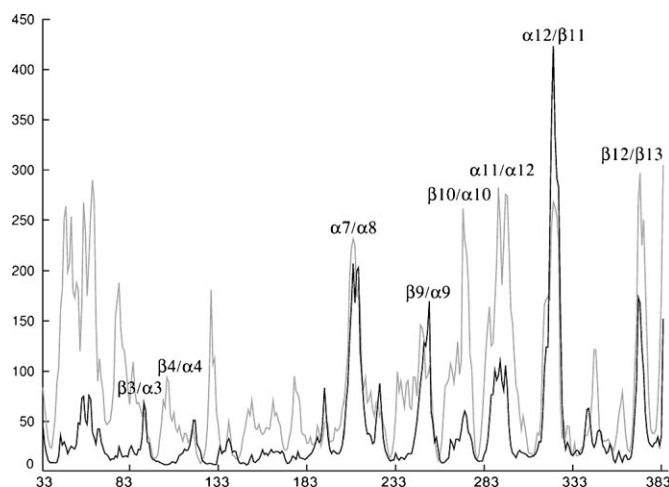

Figure 8. Amino acid residue B-values calculated from mass-weighted aver-aged backbone atom positional fluctuations of the open (gray) and closed (black) forms of the R1-R2 domain. The open form exhibits significantly higher conformational flexibility than the closed one. The most flexible parts of the protein are labelled.

estingly, MD simulations gave results which were similar to what was already seen during the homology modeling proce-dure. Apart from the α7/α8 region which is found to be com-paratively flexible only in the MD calculations, the degree of flexibility suggested by the homology modeling and MD simu-lations is similar. Moreover if comparing the protein motion

during the simulation in the open and closed conformations of NR2B it is evident that the open form displays a higher degree of protein flexibility if compared to the closed one as already observed for the homology modeling results.

The absence of large protein conformational rearrangements during the unrestrained MD simulation is certainly an indica-tion of the accuracy in the prediction of the protein folding and supports the feasibility of the proposed sequence align-ment. Moreover, the stability of the structures for at least a nanosecond after several hundred picoseconds of equilibration and the conservation of the overall structures of both the open and closed receptor conformations also suggests that a stable conformational equilibrium was reached in all cases which is a prerequisite for performing MM-PBSA calculations.

Notably, no explicit opening or closing motion of the bind-ing pockets was seen in the simulation, regardless of ligand occupancy, but it is well known that such large protein confor-mational changes are rarely observed on the timescale accessi-ble to molecular dynamics simulations. However, a working model for the opening/closing mechanism of R1-R2 could be obtained in a future study by a targeted molecular dynamics simulation speeding up the conformational change by the use of an additional biasing potential.

The binding modes of the ligand in the closed complex was found to be stable once the whole complex stabilized and the essential ligand–receptor interactions were almost all main-tained during the whole length of the simulation (Figure 9 a). At the end of the MD trajectory, the ligand position had an
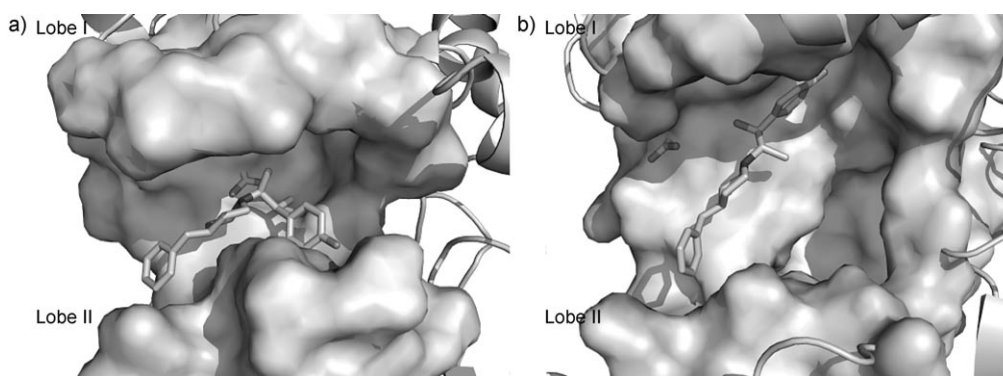
Figure 9. Energy-minimized average structures of a) closed and b) open complexes resulting from unrestrained MD calculations. In the closed cleft conformation, ifenprodil remains completely engulfed by the ligand binding site residues, whereas in the open cleft conformation, the ligand seems not to engage in stable interactions and is mostly exposed to the solvent.

RMSD value of approximately 3 Å compared to the initial pose. Basically, the main changes in the ligand conformation occur because of a rearrangement of the neighboring loops α1-β1 and β7-α7 located on the top and at the bottom of the binding site, respectively. In comparison, the RMSD of the ligand position in the open complex continues to slowly rise even after a stable protein structure was reached, up to 7 Å at the end of the MD run. In particular, a visual inspection of the frames of the MD trajectory reveals that, after 50 ps, ifenprodil changes its binding mode compared to the starting one. In fact, the orientation of the ligand switches from a perpendicular to a parallel orientation with respect to the hinge segments (Figure 9b). However, the new ligand-binding orientation proves to be rather unstable during the remaining part of the simulation and no persistent protein–ligand H-bonds were found in the open complex.

MM-PBSA calculations were performed on the ensembles of structural snapshots from the MD simulations to calculate binding free energies of ifenprodil to both the open and closed conformations of the protein. As mentioned above, the receptors, the complexes, and ifenprodil alone both in the open and closed forms of the protein were taken into account in these calculations. Actually, in these simulations it would not have been strictly necessary to conduct separate calculations for the ligand in the open and closed conformations, because both simply represent the ligand in water. However, to avoid any bias due to insufficient sampling, ligand starting conformations were taken from both complexes. The very similar results obtained for the free energies (Table 5) of the two ligand simulations make it seem likely that at least for the pure ligand sufficient sampling was accomplished.

As structural snapshots for the MM-PBSA calculations were taken from independent MD simulations of the complex, receptor, and ligand species (the three-trajectory MM-PBSA approach), small induced fit conformational changes upon ligand binding were taken into account. These calculations resulted in a $\Delta G'_{Bind}$ of -42.1 kcal mol^{-1} for binding to the closed and a $\Delta G'_{Bind}$ of -25.9 kcal mol^{-1} for binding to the open conformation. If one takes into account that no entropy correction was performed for both values and considering that such a correc-

Table 5. Calculated absolute free energies and binding free energies for ifenprodil–NMDA complexes.

Conformation	Compd	G' [kcal mol^{-1}][a]	$\Delta G'_{Bind}$ acc. to (20) [kcal mol^{-1}]
closed	complex	−5416.0	
	receptor	−5411.3	−42.1
	ligand	37.4	
open	complex	−5347.3	
	receptor	−5357.3	−25.9
	ligand	35.9	

[a] Absolute free energies and binding free energies for ifenprodil–NMDA complexes were calculated as averages over an ensemble of 100 structural snapshots taken from MD simulations. The prime indicates that no entropy correction was performed for the binding free energy. All free energies are given relative to an arbitrary zero.

tion would be approximately in the range of 20–25 kcal mol^{-1} (judged by an estimate of the ligand's rotational and translational entropy which would be lost upon binding), the result translates to the prediction of strong binding of the ligand in the closed and weak to no binding in the open conformation. A $\Delta\Delta G_{Bind}$ of 16.2 kcal mol^{-1}.

Repeating the MM-PBSA calculations using the more approximate generalized Born solvation model parametrized as described in reference [25], instead of a Poisson–Boltzmann solver to calculate the solvation free energies, yielded free energies of $+8.0$ kcal mol^{-1} for the closed and $+23.5$ kcal mol^{-1} for the open conformations, indicating no binding at all. Interestingly, the $\Delta\Delta G_{Bind}$ of 15.5 kcal mol^{-1} is in good agreement with the one from the more rigorous calculation above, meaning that relative free energies calculated using the generalized Born model can be more reliable than absolute ones.

In conclusion, the MM-PBSA results indicate that the ligand strongly binds to the closed conformation of the R1-R2 domain and a profound stabilization of the closed form occurs. On the other hand, weak or no binding was observed for ifenprodil to the open conformation of the R1-R2 domain.

Conclusions

Recent studies have shown that as regards NMDA receptors, the NTD of subunit NR2B modulates ion channel gating through the binding of extracellular allosteric modulators, such as the endogenous Zn^{2+}[11] or synthetic compounds such as ifenprodil. Recently, the ifenprodil binding site has been mapped to the LIVBP-like domain, also known as VFTM (Venus flytrap module) of the NR2B subunit and a number of key residues were found to control ifenprodil inhibition. As a result of the lack of a crystallographic structure, a combination of most available experimental data and modeling tools, such as sequence alignment, homology modeling, docking, MD simulations, and MM-PBSA was used to better understand the 3D structure of the R1-R2 domain, its interactions with ifenprodil, and its dynamics.

The evaluation of the docking results in the open and closed cleft conformations of R1-R2 domain based on ifenprodil–NR2B functional studies and ligand SARs clearly indicates that the high affinity binding site for ifenprodil is constituted by the close conformation of the NR2B R1-R2 domain. A further support to this finding comes from unrestrained MD simulations of the ifenprodil bound to the open and closed conformation of R1-R2. A first observation concerning the MD simulations, is that both complexes showed a high stability of the secondary structures (β-sheet, α-helices), thus demonstrating the correctness of the structure prediction and in turn the consistency of the HCA alignment. Over the MD simulations, neither the open complex nor the open receptor alone show any signs of closure. The same is true for the closed complex, which does not change towards an open conformation. However, monitoring the ifenprodil binding to the cleft-open conformation, a continuous instability of the ligand position was found. Over all the MD simulations, the ligand seems to be very exposed to the solvent instead of being tightly bound to the R1-R2 domain. In contrast, in the cleft-closed conformation, after the equilibration phase, the complex turned out to be very stable and ifenprodil remains completely engulfed by the ligand-binding site residues. The MM-PBSA results indicate that the ligand strongly binds to the closed conformation of the R1-R2 domain and a profound stabilization of the closed form occurs. On the other hand, a weak (or no binding, if MM-PBSA calculations with the generalized Born solvation model parametrized as described in reference [25] were used) binding was observed for ifenprodil to the open conformation of the R1-R2 domain. All considered, our studies add much strength to the hypothesis that the high affinity binding site for ifenprodil would be represented by the closed conformation of the R1-R2 domain of NR2B subunit. From our calculations, it seems more likely that ifenprodil bind directly to the closed form, shifting the equilibrium dynamic between open–closed conformations, towards the closed form through a profound stabilization of the latter. Thus, our study suggests that it may be convenient to target the closed conformation of the R1-R2 domain, rather than the open one, in the design process of new NR2B-selective antagonists. Thus, the developed model of ifenprodil–R1-R2 (closed conformation) could on one hand provide valuable hints for design of NR2B-selective antagonists and on the other could be used for virtual screening (VS) experiments. Experiments aimed to the optimization of the VS performance in the case of R1-R2 domain are in progress in our lab.

Experimental Section

Sequence alignment. The three-dimensional structure of the NR2B modulatory or regulatory domain (R1-R2) was modeled by homology to the LIVBP-like domain of the mGluR1 structure according to the sequence alignment performed by Paoletti et al.[8] and shown in Figure 2. Briefly, for the *E. coli* LIVBP[13] (PDB code: 2LIV) and rat mGluR1[14] (PDB code:1EWK), the sequence alignment was obtained from three-dimensional structure superimposition, whereas the NR2B sequence was aligned to the LIVBP-like domain of mGluR1 (18% identity), and to LIVBP (16% identity) taking into account the conserved secondary structure pattern (alternative motifs of β strands and α helices) previously detected using hydrophobic cluster analysis (HCA).[10]

Using the HCA-based sequence alignment, 3D models of the N-terminal modulatory domain of NR2B subunit (R1-R2) were built employing the MODELLER software (version 8.1) using the model-default options and setting the index of the last model to twenty.[26]

MODELLER generates protein 3D structures by satisfying spatial restraints imposed by the sequence alignment with the template structure. To guarantee sufficient conformational sampling of each binding-site residue, several homology models can be generated in this step. Preliminary tests showed that a number between 10 and 100 models provides a satisfactory sampling.[26] To optimize the local interactions, all models obtained were subjected to a short simulated annealing refinement protocol available in MODELLER.

The X-ray crystal structure of the liganded form of rat mGluR1 receptor (PDB coordinates 1EWK) was used as the structural template. Within the dimeric crystal structure, an open and a closed conformation were found, both in complex with the glutamate. Thus, protomer A and B of 1EWK were used to generate two sets of twenty models for the closed and the open conformations of the NR2B modulatory domain, respectively. All generated models were then analyzed to evaluate the structural differences among them. Finally, ten structurally nonredundant models were chosen for the open conformation and ten for the closed conformation for the subsequent ligand docking studies.

Molecular docking studies. Ifenprodil structure, with a *threo* stereochemistry and with a (1*S*,2*S*)- absolute configuration was built using the standard fragment library of the SYBYL7.2 software.[27] The initial structure was geometrically optimized and energetically minimized employing the SYBYL/MAXIMIN2 minimizer by applying the BFGS algorithm with a convergence criterion of 0.01 kcal mol^{-1}. Partial atomic charges were assigned using Gasteiger and Marsili formalism[28] as implemented in the SYBYL package. Molecular docking calculations were performed with ifenprodil in its N-protonated form, and with the piperidine ring in the chair conformation. All flexible torsions of the ligand were taken into account during the docking simulation.

Ifenprodil was docked one at a time in the ten homology models for the open and closed form, respectively. Docking studies were carried out using the AutoDock program package version 3.0.5.[29] Each homology model was set up for docking as follows: the un-

polar hydrogens were removed and Kollman united-atom partial charges were assigned. Solvation parameters were added to the receptor using the ADDSOL utility of the AutoDock program. The grid maps were calculated with AutoGrid. The grids were chosen to be large enough to include the entire interdomain crevice, and the center of the grid was set to be coincident with the D101 residue thought to be a primary anchor point for ifenprodil binding based on mutagenesis data.[10] Grid maps with $61 \times 61 \times 61$ points with a grid-point spacing of 0.375 Å were used.

In the docking simulations, the LGA algorithm, as implemented in the AutoDock program, was used applying a protocol with a maximum number of 1.5×10^6 energy evaluations, a mutation rate of 0.01, a crossover rate of 0.80, and an elitism value of 1. For the local search, the pseudo-Solis and Wets algorithm was applied using a maximum of 300 interactions per local search. In each NR2B model, fifty independent docking runs were carried out. Results differing by less than 1.5 Å in positional root-mean-square deviation (RMSD) were clustered together and represented by the result with the most favorable free energy of binding.

MD and MM-PBSA calculations. All MD simulations were performed using the amber9 suite of molecular modeling programs.[30] Force field parameters used were taken from the *ff03*[31] and *gaff*[32] forcefields included with the amber9 molecular dynamics package, for the protein parts of the system and the ligands respectively. The TIP3P[33] model for water molecules was used. Ligand partial charges were determined with the RESP methodology[34] using *Gaussian 03*[35] for quantum mechanical calculations on the HF/6–31G* level. No new forcefield parameters needed to be developed.

Six different systems were set up for MD simulations: the two receptor structures used for docking calculations (open and closed), the two complexes with ifenprodil obtained from docking calculations, and two ligand structures in its predicted binding conformations. All structures were solvated in a 12 Å layer of water molecules and neutralized using Na^+ or in the case of the ligands Cl^- ions. Prior to structural equilibration the systems were subjected to the following relaxation protocol:
– 1000 steps of steepest descent minimization with 10 kcal mol^{-1} Å^2 harmonic restraints on all solute atoms to remove steric clashes;
– 50 ps of constant volume temperature equilibration in which the system temperature was raised from 50 K to 300 K over 30 ps and held at 300 K for 20 ps by a Berendsen type coupling algorithm,[36] with harmonic restraints as above;
– 100 ps of density equilibration in the NPT ensemble at 300 K with harmonic restraints during the first 50 ps.

Equilibration was concluded by 400 ps to 1 ns structural equilibration MD simulations. These were followed by 1 ns production runs for all systems. In all MD simulations a time step of 2 fs was used, in combination with the SHAKE[37] algorithm to constrain bond lengths involving hydrogen atoms.

For MM-PBSA calculations (see ref. [38] for details of the method), structural snapshots of the different systems taken from the MD simulations were stripped of water molecules and counter ions and their absolute free energies (with respect to an arbitrary zero point) were calculated by:

$$G' = E_{FF} + G^0_{PB} + G^0_{SA} \qquad (1)$$

in which E_{FF} stands for the forcefield energy, G^0_{PB} the electrostatic part of the solvation free energy obtained by solving the Poisson–Boltzmann equation and G^0_{SA} for the nonpolar contribution to the solvation free energy, estimated by a simple empirical model

based on the surface accessible area of the solute. The prime indicates that $\Delta G'$ is not a true free energy, because no estimate of the solute entropy is included in (1). Free energies for complex, receptor, and ligand species were obtained by averaging over the different snapshots and binding free energies both for the open and closed conformations were calculated by:

$$\Delta G = G_{complex} - \left(G_{receptor} + G_{ligand} \right) \qquad (2)$$

again without a consideration of the entropy contribution to binding that results from the loss of rotational and translational degrees of freedom.

[1] a) R. Dingledine, K. Borges, D. Bowie, S. F. Traynelis, *Pharmacol. Rev.* **1999**, *51*, 7–62; b) M. L. Mayer, N. Armstrong, *Annu. Rev. Physiol.* **2004**, *66*, 161–181.

[2] a) G. L. Collingridge, W. Singer, *Trends Pharmacol. Sci.* **1990**, *11*, 290–296; b) L. Kaczmarek, M. Kossut, J. Skangiel-Kramska, *Physiol. Rev.* **1997**, *77*, 217–255; c) T. V. P. Bliss, G. L. Collingridge, *Nature* **1993**, *361*, 31–39.

[3] a) C. X. Wang, A. Shuaib, *Curr. Drug Targets: CNS Neurol. Disord.* **2005**, *4*, 143–151; b) K. Steece-Collier, L. K. Chambers, S. S. Jaw-Tsai, F. S. Menniti, J. T. Greenamyre, *Exp. Neurol.* **2000**, *163*, 239–243; c) L. Li, M. Fan, C. D. Icton, N. Chen, B. R. Leavitt, M. R. Hayden, T. H. Murphy, L. Raymond, *Neurobiol. Aging* **2003**, *24*, 1113–1121; d) L. Li, T. H. Murphy, M. R. Hayden, L. A. Raymond, *J. Neurophysiol.* **2004**, *92*, 2738–2746; e) W. Guo, F. Wei, S. Zou, M. T. Robbins, S. Sugiyo, T. Ikeda, J. C. Tu, P. F. Worley, R. Dubner, K. Ren, *J. Neurosci.* **2004**, *24*, 9161–9173; f) K. R. Gogas, *Curr. Opin. Pharmacol.* **2006**, *6*, 68–74.

[4] B. Laube, J. Kuhse, H. Betz, *J. Neurosci.* **1998**, *18*, 2954–2961.

[5] a) N. Brose, G. P. Gasic, D. E. Vetter, J. M. Sullivan, S. F. Heinemann, *J. Biol. Chem.* **1993**, *268*, 22663–22671; b) E. Meddows, B. Le Bourdelles, S. Grimwood, K. Wafford, S. Sandhu, P. Whiting, R. A. McIlhinney, *J. Biol. Chem.* **2001**, *276*, 18795–18803; c) T. Priestley, P. Laughton, J. Myers, B. Le Bourdelles, J. Kerby, P. J. Whiting, *Mol. Pharmacol.* **1995**, *48*, 841–848.

[6] R. J. Hargreaves, R. G. Hill, L. L. Iversen, *Acta. Neurochir. Suppl.* **1994**, *60*, 15–19.

[7] K. Williams, *Mol. Pharmacol.* **1993**, *44*, 851–859.

[8] a) P. J. O'Hara, P. O. Sheppard, H. Thogersen, D. Venezia, B. A. Haldeman, V. McGrane, K. M. Houamed, C. Thomsen, T. L. Gilbert, E. R. Mulvihill, *Neuron* **1993**, *11*, 41–52; b) P. Paoletti, F. Perin-Dureau, A. Fayyazuddin, A. Le Goff, .I Callebaut, Neyton, *Neuron* **2000**, *28*, 911–925.

[9] Y. Stern-Bach, B. Bettler, M. Hartley, P. O. Sheppard, P. J. O'Hara, S. F. Heinemann, *Neuron* **1994**, *13*, 1345–1357.

[10] a) P. Paoletti, F. Perin-Dureau, A. Fayyazuddin, A. Le Groff, I. Callebaut, J. Neyton, *Neuron* **2000**, *28*, 911–925; b) F. Perin-Dureau, J. Rachline, J. Neyton, P. Paoletti, *J. Neurosci.* **2002**, *22*, 5955–5965; c) P. Malherbe, V. Mutel, C. Broger, F. Perin-Dureau, J. A. Kemp, J. Neyton, P. Paoletti, J. N. Kew. , *J. Pharmacol. Exp. Ther.* **2003**, *307*, 897–905.

[11] J. Rachline, F. Perin-Dureau, A. Le Goff, J. Neyton, P. Paoletti, *J. Neurosci.* **2005**, *25*, 308–317.

[12] Y. Paas, A. Devillers-Thiéry, V. I. Teichberg, J. P. Changeux, M. Eisenstein, *Trends Pharmacol. Sci.* **2000**, *21*, 87–92.

[13] a) J. S. Sack, M. A. Saper, F. A. Quiocho, *J. Mol. Biol.* **1989**, *206*, 171–191; b) S. Trakhanov, N. K. Vyas, H. Luecke, D. M. Kristensen, J. Ma, F. A. Quiocho, *Biochemistry* **2005**, *44*, 6597–6608.

[14] N. Kunishima, Y. Shimada, Y. Tsuji, T. Sato, M. Yamamoto, T. Kumasaka, S. Nakanishi, H. Jingami, K. Morikawa, *Nature* **2000**, *407*, 971–977.

[15] M. J. Gallagher, H. Huang, D. B. Pritchett, D. R. Lynch, *J. Biol. Chem.* **1996**, *271*, 9603–9611.

[16] T. Masuko, K. Kashiwagi, T. Kuno, N. D. Nguyen, A. J. Pahk, J. Fukuchi, K. Igarashi, K. A. Williams, *Mol. Pharmacol.* **1999**, *55*, 957–969.

[17] X. L. He, D. C. Chow, M. M. Martick, K. C. Garcia, *Science* **2001**, *293*, 1657–1662.

[18] P. Avenet, J. Leonardon, F. Besnard, D. Graham, J. Frost, H. Depoortere, S. Z. Langer, B. Scatton, *Eur. J. Pharmacol.* **1996**, *296*, 209–213.

[19] B. L. Chenard, I. A. Shalaby, B. K. Koe, R. T. Ronau, T. W. Butler, M. A. Prochniak, A. W. Schmidt, C. B. Fox, *J. Med. Chem.* **1991**, *34*, 3085–3090.

[20] B. L. Chenard, J. Bordner, T. W. Butler, L. K. Chambers, M. A. Collins, D. L. De Costa, M. F. Ducat, M. L. Dumont, C. B. Fox, E. E. Mena, F. S. Menniti, J. Nielsen, M. J. Pagnozzi, K. E. G. Richter, R. T. Ronau, I. A. Shalaby, J. Z. Stemple, W. F. White, *J. Med. Chem.* **1995**, *38*, 3138–3145.

[21] B. L. Chenard, I. A. Shalaby, B. K. Koe, R. T. Ronau, T. W. Butler, M. A. Prochniak, A. W. Schmidt, C. B. Fox, *J. Med. Chem.* **1991**, *34*, 3085–3090.

[22] I. Borza, G. Domany, *Curr. Top. Med. Chem.* **2006**, *6*, 687–695.

[23] A. P. Tamiz, E. R. Whittemore, Z. L. Zhou, J. C. Huang, J. A. Drewe, J. C. Chen, S. X. Cai, E. Weber, R. M. Woodward, J. F. W. Keana, *J. Med. Chem.* **1998**, *41*, 3499–3506.

[24] a) M. E. Layton, M. J. Kelly III, K. J. Rodzinak, *Curr. Top. Med. Chem.* **2006**, *6*, 697–709; b) I. Borza, G. Domány, *Curr. Top. Med. Chem.* **2006**, *6*, 687–695.

[25] V. Tsui, D. A. Case, *Biopolymers* **2000**, *56*, 275–291.

[26] a) M. A. Marti-Renom, A. C. Stuart, A. Fiser, R. Sanchez, F. Melo, A. Sali, *Annu. Rev. Biophys. Biomol. Struct.* **2000**, *29*, 291–325; b) A. Sali, T. L. Blundell, *J. Mol. Biol.* **1993**, *234*, 779–815.

[27] SYBYL Molecular Modelling System, version 6.9.1; Tripos Inc.: St. Louis, MO, **2003**.

[28] J. Gasteiger, M. Marsili, *Tetrahedron* **1980**, *36*, 3219–3228.

[29] a) G. M. Morris, D. S. Goodsell, R. S. Halliday, R. Huey, W. E. Hart, R. K. Belew, A. J. Olson, *J. Comput. Chem.* **1998**, *19*, 1639–1662, (The Scripps Research Institute, La Jolla, CA 92037–1000); b) D. S. Goodsell, G. M. Morris, A. J. Olson, *J. Mol. Recognit.* **1996**, *9*, 1–5.

[30] D. A. Case, T. A. Darden, T. E. Cheatham III, C. L. Simmerling, J. Wang, R. E. Duke, R. Luo, K. M. Merz, B. Wang, D. A. Pearlman, M. Crowley, S. Brozell, V. Tsui, H. Gohlke, J. Mongan, V. Hornak, G. Cui, P. Beroza, C. Schafmeister, J. W. Caldwell, W. S. Ross, P. A. Kollman. *AMBER 9*, University of California, San Francisco, **2004**.

[31] Y. Duan, C. Wu, S. Chowdhury, M. C. Lee, G. Xiong, W. Zhang, R. Yang, P. Cieplak, R. Luo, T. Lee, J. Caldwell, J. Wang, P. A. Kollman, *J. Comput. Chem.* **2003**, *24*, 1999–2012.

[32] J. Wang, R. M. Wolf, J. W. Caldwell, P. A. Kollman, D. A. Case, *J. Comput. Chem.* **2004**, *25*, 1157–1174.

[33] W. L. Jorgensen, J. Chandrasekhar, J. D. Madura, R. W. Impey, M. L. Klein, *J. Chem. Phys.* **1983**, *79*, 926–935.

[34] C. I. Bayly, P. Cieplak, W. Cornell, P. A. Kollman, *J. Phys. Chem.* **1993**, *97*, 10269–10280.

[35] Gaussian 03, Revision C.02, M. J. Frisch, G. W. Trucks, H. B. Schlegel, G. E. Scuseria, M. A. Robb, J. R. Cheeseman, Jr., J. A. Montgomery, T. Vreven, K. N. Kudin, J. C. Burant, J. M. Millam, S. S. Iyengar, J. Tomasi, V. Barone, B. Mennucci, M. Cossi, G. Scalmani, N. Rega, G. A. Petersson, H. Nakatsuji, M. Hada, M. Ehara, K. Toyota, R. Fukuda, J. Hasegawa, M. Ishida, T. Nakajima, Y. Honda, O. Kitao, H. Nakai, M. Klene, X. Li, J. E. Knox, H. P. Hratchian, J. B. Cross, V. Bakken, C. Adamo, J. Jaramillo, R. Gomperts, R. E. Stratmann, O. Yazyev, A. J. Austin, R. Cammi, C. Pomelli, J. W. Ochterski, P. Y. Ayala, K. Morokuma, G. A. Voth, P. Salvador, J. J. Dannenberg, V. G. Zakrzewski, S. Dapprich, A. D. Daniels, M. C. Strain, O. Farkas, D. K. Malick, A. D. Rabuck, K. Raghavachari, J. B. Foresman, J. V. Ortiz, Q. Cui, A. G. Baboul, S. Clifford, J. Cioslowski, B. B. Stefanov, G. Liu, A. Liashenko, P. Piskorz, I. Komaromi, R. L. Martin, D. J. Fox, M. A. Keith, Al-Laham, C. Y. Peng, A. Nanayakkara, M. Challacombe, P. M. W. Gill, B. Johnson, W. Chen, M. W. Wong, C. Gonzalez, J. A. Pople, Inc Gaussian, C. T. Wallingford, **2004**.

[36] H. J. C. Berendsen, J. P. M. Postma, W. F. van Gunsteren, A. Di Nola, J. R. Haak, *J. Chem. Phys.* **1984**, *81*, 3684–3690.

[37] J. P. Ryckaert, G. Ciccotti, H. J. C. Berendsen, *J. Comput. Phys.* **1977**, *23*, 327–341.

[38] a) P. A. Kollman, I. Massova, C. Reyes, B. Kuhn, S. Huo, L. Chong, M. Lee, T. Lee, Y. Duan, W. Wang, O. Donini, P. Cieplak, J. Srinivasan, D. A. Case, T. E. Cheatham III, *Acc. Chem. Res.* **2000**, *33*, 889–897; b) J. Srinivasan, T. E. Cheatham III, P. Cieplak, P. A. Kollman, D. A. Case, *J. Am. Chem. Soc.* **1998**, *120*, 9401–9409; c) H. Ni, C. A. Sotriffer, J. A. McCammon, *J. Med. Chem.* **2001**, *44*, 3043–3047.